## SUPPLEMENTARY MATERIALS

# Evidence for syngenetic micro-inclusions of $As^{3+}$- and $As^{5+}$-containing Cu sulfides in hydrothermal pyrite

Margarita Merkulova*, Magdalena Murdzek, Olivier Mathon, Pieter Glatzel, Valentina Batanova, Alain Manceau

**Table S1.** EPMA analyses of pyrite.

| At 20 kV accelerating voltage and 20 nA beam current | | | | | | | | | | | | |
|---|---|---|---|---|---|---|---|---|---|---|---|---|
| | Fe | S | Zn | Cu | Sb | Te | Bi | As | V | Sn | Co | Total |
| D.L. | 0.01 | 0.04 | 0.03 | 0.02 | 0.02 | 0.03 | 0.05 | 0.01 | 0.01 | 0.02 | | |
| 1P | 46.74 | 53.98 | b.d.l. | b.d.l. | b.d.l. | b.d.l. | b.d.l. | b.d.l. | b.d.l. | b.d.l. | n.a. | 100.77 |
| | 46.64 | 54.21 | b.d.l. | b.d.l. | b.d.l. | b.d.l. | b.d.l. | b.d.l. | b.d.l. | b.d.l. | n.a. | 100.85 |
| | 46.61 | 53.94 | b.d.l. | b.d.l. | b.d.l. | b.d.l. | b.d.l. | b.d.l. | b.d.l. | b.d.l. | n.a. | 100.56 |
| | 46.65 | 54.17 | b.d.l. | b.d.l. | b.d.l. | b.d.l. | b.d.l. | b.d.l. | b.d.l. | b.d.l. | n.a. | 100.83 |
| | 46.51 | 54.01 | b.d.l. | b.d.l. | b.d.l. | b.d.l. | b.d.l. | b.d.l. | b.d.l. | b.d.l. | n.a. | 100.55 |
| | 46.56 | 53.73 | b.d.l. | b.d.l. | b.d.l. | b.d.l. | b.d.l. | b.d.l. | b.d.l. | b.d.l. | n.a. | 100.35 |
| | 46.65 | 54.08 | b.d.l. | b.d.l. | b.d.l. | b.d.l. | b.d.l. | b.d.l. | b.d.l. | b.d.l. | n.a. | 100.76 |
| 2P | 46.52 | 54.18 | b.d.l. | b.d.l. | b.d.l. | b.d.l. | b.d.l. | b.d.l. | b.d.l. | b.d.l. | n.a. | 100.74 |
| | 46.56 | 54.16 | b.d.l. | b.d.l. | b.d.l. | b.d.l. | b.d.l. | b.d.l. | b.d.l. | b.d.l. | n.a. | 100.77 |
| | 46.58 | 54.03 | b.d.l. | b.d.l. | b.d.l. | b.d.l. | b.d.l. | b.d.l. | b.d.l. | b.d.l. | n.a. | 100.63 |
| | 46.74 | 54.18 | b.d.l. | b.d.l. | b.d.l. | b.d.l. | b.d.l. | b.d.l. | b.d.l. | b.d.l. | n.a. | 100.97 |
| | 46.56 | 53.99 | b.d.l. | b.d.l. | b.d.l. | b.d.l. | b.d.l. | b.d.l. | b.d.l. | b.d.l. | n.a. | 100.58 |
| | 46.72 | 53.82 | b.d.l. | b.d.l. | b.d.l. | b.d.l. | b.d.l. | b.d.l. | b.d.l. | b.d.l. | n.a. | 100.57 |
| | 46.72 | 53.98 | b.d.l. | b.d.l. | b.d.l. | b.d.l. | b.d.l. | b.d.l. | b.d.l. | b.d.l. | n.a. | 100.72 |
| 3P | 46.73 | 53.86 | b.d.l. | b.d.l. | b.d.l. | b.d.l. | b.d.l. | b.d.l. | b.d.l. | b.d.l. | n.a. | 100.62 |
| | 46.61 | 53.95 | b.d.l. | b.d.l. | b.d.l. | b.d.l. | b.d.l. | b.d.l. | b.d.l. | b.d.l. | n.a. | 100.61 |
| | 46.66 | 53.84 | b.d.l. | b.d.l. | b.d.l. | b.d.l. | b.d.l. | b.d.l. | b.d.l. | b.d.l. | n.a. | 100.52 |
| | 46.39 | 54.01 | b.d.l. | b.d.l. | b.d.l. | b.d.l. | b.d.l. | b.d.l. | b.d.l. | b.d.l. | n.a. | 100.42 |
| | 46.31 | 54.19 | b.d.l. | b.d.l. | b.d.l. | b.d.l. | b.d.l. | b.d.l. | b.d.l. | b.d.l. | n.a. | 100.68 |
| | 46.52 | 54.04 | b.d.l. | b.d.l. | b.d.l. | b.d.l. | b.d.l. | b.d.l. | b.d.l. | b.d.l. | n.a. | 100.59 |
| | 46.53 | 54.08 | b.d.l. | b.d.l. | b.d.l. | b.d.l. | b.d.l. | b.d.l. | b.d.l. | b.d.l. | n.a. | 100.63 |
| At 20 kV accelerating voltage and 900 nA beam current | | | | | | | | | | | | |
| | Fe | S | Zn | Cu | Sb | Te | Bi | As | V | Sn | Co | Total |
| D.L. | | | | 0.002 | | | | 0.002 | | | 0.003 | |
| 1P | 46.64 | 53.75 | n.a. | 0.002 | n.a. | n.a. | n.a. | 0.003 | n.a. | n.a. | 0.005 | 100.42 |
| | 46.55 | 54.21 | n.a. | 0.002 | n.a. | n.a. | n.a. | 0.005 | n.a. | n.a. | 0.009 | 100.80 |
| | 46.54 | 53.73 | n.a. | 0.009 | n.a. | n.a. | n.a. | 0.000 | n.a. | n.a. | 0.006 | 100.30 |
| 2P | 46.47 | 53.45 | n.a. | 0.003 | n.a. | n.a. | n.a. | 0.003 | n.a. | n.a. | 0.008 | 99.94 |
| | 46.51 | 53.37 | n.a. | 0.004 | n.a. | n.a. | n.a. | 0.004 | n.a. | n.a. | 0.006 | 99.92 |
| | 46.67 | 53.27 | n.a. | 0.005 | n.a. | n.a. | n.a. | 0.000 | n.a. | n.a. | 0.006 | 99.98 |
| | 46.62 | 53.39 | n.a. | 0.004 | n.a. | n.a. | n.a. | 0.000 | n.a. | n.a. | 0.007 | 100.03 |
| 3P | 46.57 | 53.31 | n.a. | 0.002 | n.a. | n.a. | n.a. | 0.000 | n.a. | n.a. | 0.005 | 99.91 |
| | 46.46 | 53.28 | n.a. | b.d.l. | n.a. | n.a. | n.a. | 0.005 | n.a. | n.a. | 0.005 | 99.76 |

*Notes:* All concentrations in wt%.
D.L. – detection limit; b.d.l. – below detection limit; n.a. – not analysed.

**Table S2.** EPMA analyses of Cu-sulfide inclusions.

| | Fe | S | Zn | Cu | Sb | Te | Bi | As | V | Sn | Total | Mineral | Chemical formula | Σ cations | Σ positive charge |
|---|---|---|---|---|---|---|---|---|---|---|---|---|---|---|---|
| D.L. | 0.01 | 0.03 | 0.04 | 0.02 | 0.02 | 0.04 | 0.05 | 0.02 | 0.01 | 0.02 | | | | | |
| 1P | 1.09 | 32.14 | b.d.l. | 48.63 | 0.87 | b.d.l. | b.d.l. | 16.77 | b.d.l. | 0.11 | 99.62 | enargite | $Cu_{3.1}Fe_{0.1}As_{0.9}S_4$ | 4.06 | 7.69 |
| | 0.93 | 32.37 | b.d.l. | 48.29 | 1.11 | b.d.l. | b.d.l. | 17.05 | b.d.l. | 0.18 | 99.93 | enargite | $Cu_3Fe_{0.1}As_{0.9}S_4$ | 4.01 | 7.63 |
| | 4.26 | 30.94 | b.d.l. | 46.06 | 1.88 | b.d.l. | b.d.l. | 7.28 | 1.95 | 6.34 | 98.70 | colusite | $(Cu_{24}Fe_{1.8})(V_{1.3}Fe_{0.7})(As_{3.2}Sb_{0.5})Sn_{1.8}S_{32}$ | 33.27 | 61.06 |
| | 3.14 | 30.96 | b.d.l. | 48.36 | 1.43 | b.d.l. | b.d.l. | 7.12 | 2.23 | 6.49 | 99.72 | colusite | $(Cu_{25.2}Fe_{0.8})(V_{1.4}Fe_{1.1})(As_{3.1}Sb_{0.4})Sn_{1.8}S_{32}$ | 33.82 | 61.01 |
| | 3.71 | 31.90 | b.d.l. | 47.93 | 2.43 | b.d.l. | b.d.l. | 6.62 | 2.21 | 7.00 | 101.81 | colusite | $(Cu_{24.2}Fe_{1.5})(V_{1.4}Fe_{0.6})(As_{2.8}Sb_{0.6})Sn_{1.9}S_{32}$ | 33.11 | 60.41 |
| | 4.56 | 31.07 | b.d.l. | 47.51 | 2.39 | b.d.l. | b.d.l. | 6.49 | 1.73 | 6.87 | 100.62 | colusite | $(Cu_{24.6}Fe_{1.4})(V_{1.1}Fe_{1.3})(As_{2.9}Sb_{0.6})Sn_{1.9}S_{32}$ | 33.86 | 60.74 |
| | 0.71 | 26.20 | 0.11 | 47.20 | 4.64 | 13.94 | 1.66 | 6.31 | b.d.l. | b.d.l. | 100.76 | As-goldfieldite | $(Cu_{11.8}Fe_{0.2})(As_{1.3}Sb_{0.6}Bi_{0.1})Te_{1.7}S_{13}$ | 15.83 | 25.39 |
| | 1.59 | 25.27 | 0.62 | 45.27 | 7.60 | 9.17 | 4.66 | 5.89 | b.d.l. | b.d.l. | 100.07 | As-goldfieldite | $(Cu_{11.7}Fe_{0.5})(As_{1.3}Sb_{1.0}Bi_{0.4})Te_{1.2}S_{13}$ | 16.22 | 25.78 |
| | 1.78 | 25.86 | 0.16 | 46.88 | 2.90 | 13.68 | 1.77 | 7.42 | b.d.l. | b.d.l. | 100.46 | As-goldfieldite | $(Cu_{11.9}Fe_{0.5})(As_{1.6}Sb_{0.4}Bi_{0.1})Te_{1.7}S_{13}$ | 16.26 | 26.21 |
| | 9.58 | 30.14 | b.d.l. | 41.68 | 1.12 | 0.06 | b.d.l. | 0.66 | 0.04 | 17.84 | 101.13 | mawsonite | $Cu_{5.6}Fe_{1.5}(Sn_{1.3}As_{0.1}Sb_{0.1})S_8$ | 8.47 | 14.36 |
| | 9.84 | 29.54 | b.d.l. | 41.19 | 0.49 | 0.09 | b.d.l. | 0.48 | 0.06 | 18.47 | 100.15 | mawsonite | $Cu_{5.6}Fe_{1.5}(Sn_{1.3}As_{0.1})S_8$ | 8.60 | 14.51 |
| 2P | 1.85 | 31.05 | 0.04 | 49.29 | 0.63 | b.d.l. | b.d.l. | 7.36 | 2.63 | 7.64 | 100.52 | colusite | $(Cu_{25.6}Fe_{0.4})(V_{1.7}Fe_{0.7})(As_{3.2}Sb_{0.2})Sn_{2.1}S_{32}$ | 33.94 | 61.88 |
| | 0.67 | 31.54 | b.d.l. | 49.93 | 0.63 | b.d.l. | b.d.l. | 8.34 | 3.19 | 6.47 | 100.79 | colusite | $(Cu_{25.5})(V_2Fe_{0.4})(As_{3.6}Sb_{0.2})Sn_{1.8}S_{32}$ | 33.48 | 62.43 |
| | 0.71 | 31.45 | b.d.l. | 50.04 | 0.56 | b.d.l. | b.d.l. | 8.21 | 2.98 | 6.48 | 100.46 | colusite | $(Cu_{25.6})(V_{1.9}Fe_{0.4})(As_{3.6}Sb_{0.2})Sn_{1.8}S_{32}$ | 33.46 | 61.69 |
| | 0.69 | 30.78 | b.d.l. | 50.32 | 0.61 | b.d.l. | b.d.l. | 8.37 | 2.95 | 6.14 | 99.88 | colusite | $(Cu_{26.3})(V_{1.9}Fe_{0.4})(As_{3.7}Sb_{0.2})Sn_{1.7}S_{32}$ | 34.29 | 63.10 |
| | 0.24 | 31.25 | b.d.l. | 50.30 | 0.35 | b.d.l. | b.d.l. | 8.71 | 3.25 | 6.22 | 100.33 | colusite | $(Cu_{25.9})(V_{2.1}Fe_{0.1})(As_{3.8}Sb_{0.1})Sn_{1.7}S_{32}$ | 33.80 | 63.08 |
| | 0.61 | 31.53 | b.d.l. | 49.96 | 0.46 | b.d.l. | b.d.l. | 9.03 | 3.24 | 5.76 | 100.59 | colusite | $(Cu_{25.5})(V_{2.1}Fe_{0.4})(As_{3.9}Sb_{0.1})Sn_{1.6}S_{32}$ | 33.57 | 63.05 |
| | 1.26 | 30.81 | b.d.l. | 49.71 | 0.44 | b.d.l. | b.d.l. | 8.12 | 3.17 | 6.39 | 99.93 | colusite | $(Cu_{26.0})(V_{2.1}Fe_{0.8})(As_{3.6}Sb_{0.1})Sn_{1.8}S_{32}$ | 34.34 | 63.63 |
| | 0.35 | 31.21 | b.d.l. | 50.29 | 0.46 | b.d.l. | b.d.l. | 8.74 | 3.19 | 6.01 | 100.29 | colusite | $(Cu_{26.0})(V_{2.1}Fe_{0.2})(As_{3.8}Sb_{0.1})Sn_{1.7}S_{32}$ | 33.84 | 63.05 |
| | 9.13 | 25.11 | b.d.l. | 65.88 | b.d.l. | b.d.l. | 0.34 | b.d.l. | b.d.l. | b.d.l. | 100.48 | bornite | $Cu_{5.3}Fe_{0.8}S_4$ | 6.13 | 6.95 |
| | 11.93 | 25.63 | b.d.l. | 61.88 | b.d.l. | b.d.l. | 0.80 | b.d.l. | b.d.l. | b.d.l. | 100.26 | bornite | $Cu_{4.9}Fe_{1.1}S_4$ | 5.95 | 7.00 |

**Table S2.** Continued.

| | Fe | S | Zn | Cu | Sb | Te | Bi | As | V | Sn | Total | Mineral | Chemical formula | Σ cations | Σ positive charge |
|---|---|---|---|---|---|---|---|---|---|---|---|---|---|---|---|
| D.L. | 0.01 | 0.03 | 0.04 | 0.02 | 0.02 | 0.04 | 0.05 | 0.02 | 0.01 | 0.02 | | | | | |
| 3P | 1.38 | 32.05 | b.d.l. | 47.99 | 0.99 | b.d.l. | b.d.l. | 17.33 | b.d.l. | 0.07 | 99.81 | enargite | $Cu_3Fe_{0.1}As_{0.9}S_4$ | 4.07 | 7.83 |
| | 5.27 | 30.43 | 0.05 | 45.88 | 1.91 | b.d.l. | b.d.l. | 4.46 | 1.67 | 11.10 | 100.78 | colusite | $(Cu_{24.3}Fe_{1.7})(V_{1.1}Fe_{1.5})(As_{2.0}Sb_{0.5})Sn_{3.1}S_{32}$ | 34.29 | 61.47 |
| | 3.17 | 30.11 | 0.06 | 47.48 | 1.90 | b.d.l. | b.d.l. | 5.41 | 2.23 | 9.79 | 100.17 | colusite | $(Cu_{25.4}Fe_{0.6})(V_{1.5}Fe_{1.3})(As_{2.5}Sb_{0.5})Sn_{2.8}S_{32}$ | 34.64 | 62.92 |
| | 0.93 | 25.09 | 0.15 | 53.21 | 3.09 | 10.86 | 0.48 | 5.08 | b.d.l. | b.d.l. | 98.90 | As-goldfieldite | $(Cu_{13.9}Fe_{0.3})(As_{1.1}Sb_{0.4})Te_{1.4}S_{13}$ | 17.19 | 24.91 |
| | 0.51 | 25.83 | 0.09 | 46.92 | 2.36 | 15.91 | 1.21 | 7.92 | b.d.l. | b.d.l. | 100.77 | As-goldfieldite | $(Cu_{11.9}Fe_{0.1})(As_{1.7}Sb_{0.3}Bi_{0.1})Te_2S_{13}$ | 16.18 | 26.59 |
| | 1.05 | 25.98 | 0.12 | 47.10 | 3.10 | 14.91 | 1.48 | 6.74 | b.d.l. | b.d.l. | 100.48 | As-goldfieldite | $(Cu_{11.9}Fe_{0.3})(As_{1.4}Sb_{0.4}Bi0.1)Te_{1.9}S_{13}$ | 16.03 | 25.90 |
| | 0.87 | 25.84 | 0.32 | 46.84 | 5.61 | 12.83 | 1.91 | 6.15 | b.d.l. | b.d.l. | 100.38 | As-goldfieldite | $(Cu_{11.9}Fe_{0.3})(As_{1.3}Sb_{0.7}Bi0.1)Te_{1.6}S_{13}$ | 16.03 | 25.63 |
| | 1.04 | 26.02 | 0.10 | 47.35 | 2.52 | 15.14 | 1.20 | 7.21 | b.d.l. | b.d.l. | 100.58 | As-goldfieldite | $(Cu_{11.9}Fe_{0.3})(As_{1.5}Sb_{0.3}Bi0.1)Te_{1.9}S_{13}$ | 16.09 | 26.03 |
| | 1.59 | 25.97 | 0.26 | 46.28 | 4.98 | 13.47 | 1.69 | 6.24 | b.d.l. | b.d.l. | 100.48 | As-goldfieldite | $(Cu_{11.7}Fe_{0.5})(As_{1.3}Sb_{0.7}Bi0.1)Te_{1.7}S_{13}$ | 15.99 | 25.83 |
| | 2.33 | 25.81 | 0.14 | 46.13 | 3.64 | 14.50 | 1.74 | 6.41 | b.d.l. | b.d.l. | 100.70 | As-goldfieldite | $(Cu_{11.7}Fe_{0.7})(As_{1.4}Sb_{0.5}Bi0.1)Te_{1.8}S_{13}$ | 16.24 | 26.43 |
| | 1.91 | 25.72 | 0.20 | 46.10 | 2.47 | 12.74 | 4.27 | 7.18 | b.d.l. | 0.03 | 100.62 | As-goldfieldite | $(Cu_{11.7}Fe_{0.6})(As_{1.6}Sb_{0.3}Bi_{0.3})Te_{1.6}S_{13}$ | 16.17 | 26.03 |
| | 2.87 | 25.67 | 0.13 | 45.33 | 1.62 | 11.68 | 5.53 | 8.02 | b.d.l. | b.d.l. | 100.85 | As-goldfieldite | $(Cu_{11.6}Fe_{0.8})(As_{1.7}Sb_{0.2}Bi_{0.4})Te_{1.5}S_{13}$ | 16.28 | 26.35 |
| | 0.38 | 26.02 | 0.22 | 47.64 | 3.66 | 14.16 | 1.49 | 6.93 | b.d.l. | b.d.l. | 100.49 | As-goldfieldite | $(Cu_{12.0}Fe_{0.1})(As_{1.5}Sb_{0.5}Bi_{0.1})Te_{1.8}S_{13}$ | 16.00 | 25.63 |
| | 2.21 | 25.63 | 0.64 | 44.73 | 8.54 | 8.37 | 3.85 | 6.16 | b.d.l. | b.d.l. | 100.14 | As-goldfieldite | $(Cu_{11.4}Fe_{0.6})(As_{1.3}Sb_{1.1}Bi_{0.3})Te_{1.1}S_{13}$ | 16.06 | 25.60 |
| | 13.37 | 29.69 | b.d.l. | 43.88 | b.d.l. | 0.05 | b.d.l. | 0.00 | 0.06 | 13.54 | 100.59 | mawsonite | $Cu_6Fe_{2.1}SnS_8$ | 9.02 | 14.02 |
| | 10.79 | 30.17 | 0.04 | 43.67 | 1.15 | 0.04 | b.d.l. | 2.96 | b.d.l. | 12.01 | 100.84 | mawsonite | $Cu_{5.8}Fe_{1.6}(Sn_{0.9}As_{0.3}Sb_{0.1})S_8$ | 8.75 | 14.62 |
| | 11.82 | 25.95 | b.d.l. | 62.02 | b.d.l. | b.d.l. | 0.12 | b.d.l. | b.d.l. | 0.02 | 99.93 | bornite | $Cu_{4.8}Fe_{1.0}S_4$ | 5.86 | 6.90 |

*Notes:* All concentrations in wt%.
D.L. – detection limit; b.d.l. – below detection limit; n.a. – not analysed.

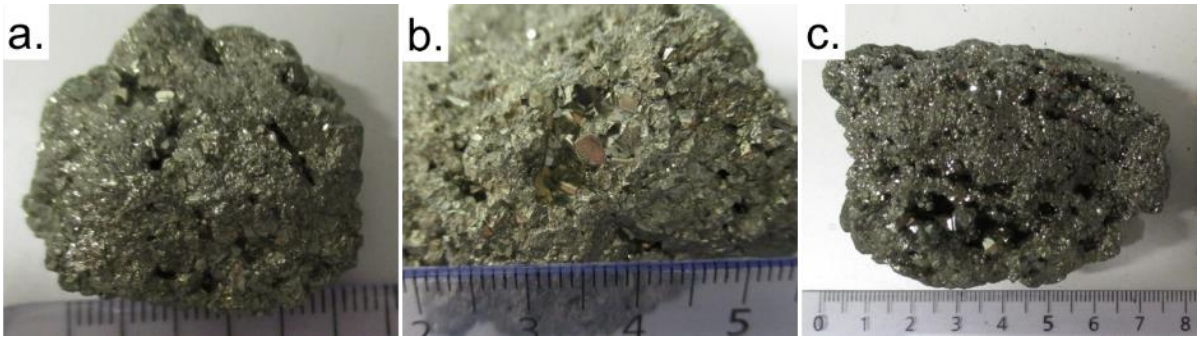


**Figure S1.** Photographs of Peruvian pyrite aggregates: (**a**) 1P, (**b**) 2P, (**c**) 3P.

**X-ray powder diffraction (XRD)**

XRD analysis was performed at ISTerre on a BrukerD8 diffractometer equipped with a selective energy detector (SolXEM, Baltics Instruments). Electron voltage and current were 40 kV and 40 mA. Intensity from the diffracted Cu Kα1 radiation was measured from 5 to 90° 2θ with a step size of 0.03° and a dwell time of 6 s per step. Full XRD patterns are shown in Fig. S2a. The 51-55° 2θ interval is zoomed in Fig. S2b to show the absence of marcasite impurity in the samples.

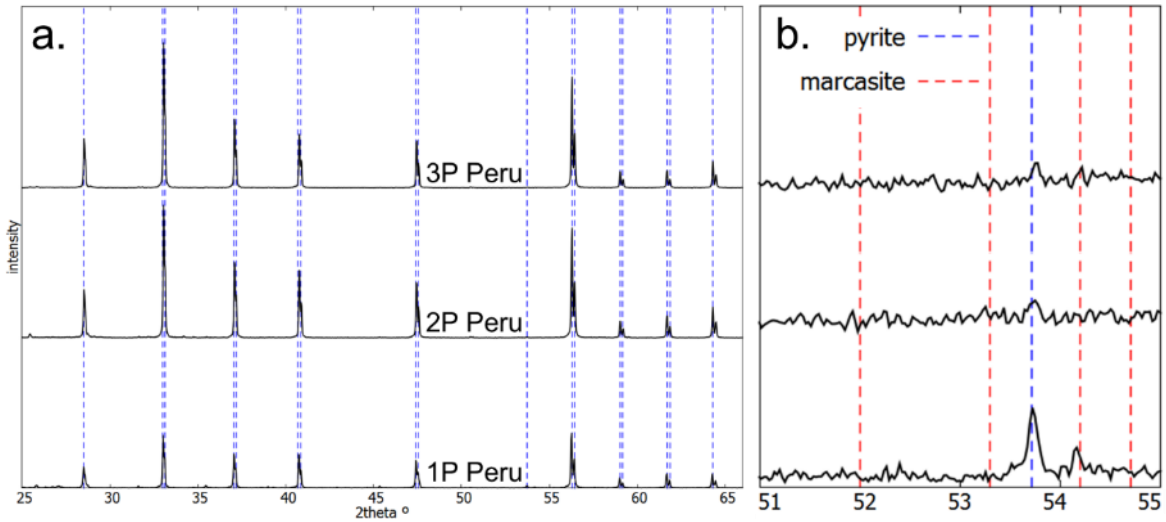


**Figure S2.** (**a**) XRD patterns of pyrite. Blue dashed lines indicate the reflections of pyrite; (**b**) Zoomed angular region. The position of the most intense reflections of marcasite are indicated.

**ICP-MS**

Trace and minor element contents were determined by inductively coupled plasma-mass spectrometry (ICP-MS) at Bureau Veritas (Canada). Samples were pulverized using a mortar and a pestle and digested in aqua regia for further analysis. Analytical code AQ270 (ICP-ES/MS) was used. Certified standard references and blanks were measured in the same conditions as the samples. Obtained concentrations are shown in Table 1.

**EPMA**

Backscattered electron (BSE) images, EPMA and elemental maps were performed with a JEOL JXA-8230 electron microprobe at ISTerre. Representative BSE images are shown in Figure 1 and Figure S3. Quantitative point analysis were acquired with five wavelength-dispersive spectrometers (WDS) and an energy-dispersive (EDS) spectrometer. Analyses were acquired with two analytical protocols. Operating conditions for the first one were 20 kV accelerating voltage and 20 nA beam current with a focused beam of 1-3 μm in diameter. The concentrations of Fe, Zn, Cu, S, Sb, Te, Bi, As, V and Sn were measured with the WDS. Operating conditions for the second protocol, used for high-precision analysis of pyrite, were 20 kV accelerating voltage and 900 nA beam current with a focused beam of 1-3 μm. In this protocol, the concentrations of As, Se, Cu, Co, and Au were measured with the WDS and those of Fe and S with the EDS. The following certified natural and synthetic materials were used for standardization: As: FeAsS; Se: Se and $Bi_2Se_3$; Au: Au; Zn: ZnS; Ni: Ni; Co: CoO; Sn: $SnO_2$; Cu: $CuFeS_2$; Fe: $CuFeS_2$ and $FeS_2$; V: V; Bi: Bi; Te: $Ag_2Te$; Sb: $Sb_2S_3$; S: $CuFeS_2$. Point analyses are listed in Table S1 and Table S2.

Electron microprobe elemental maps were acquired for As, Fe, S, Cu, Se, Au, Pb, Bi, and V (Figs. S4 and S5). Fe, S, Bi, V were analyzed by EDS and As, Se, Au, Pb by WDS. The spot and step sizes were 1 or 2 μm, the electron voltage 20 kV and current 500 nA, and the dwell time 500 to 1000 ms.

In the three mapped regions represented in Figures S4 and S5, As shows higher concentration in the 1P and 3P inclusions and lower in the 2P inclusion (Fig. S4). The 2P inclusion is bornite, which has no As (Table S2). The 1P and 3P inclusions are depleted in Bi but have higher V content than pyrite. This composition is characteristic of colusite. The pyrite crystals contain Au, Pb, Se, Bi, and V.

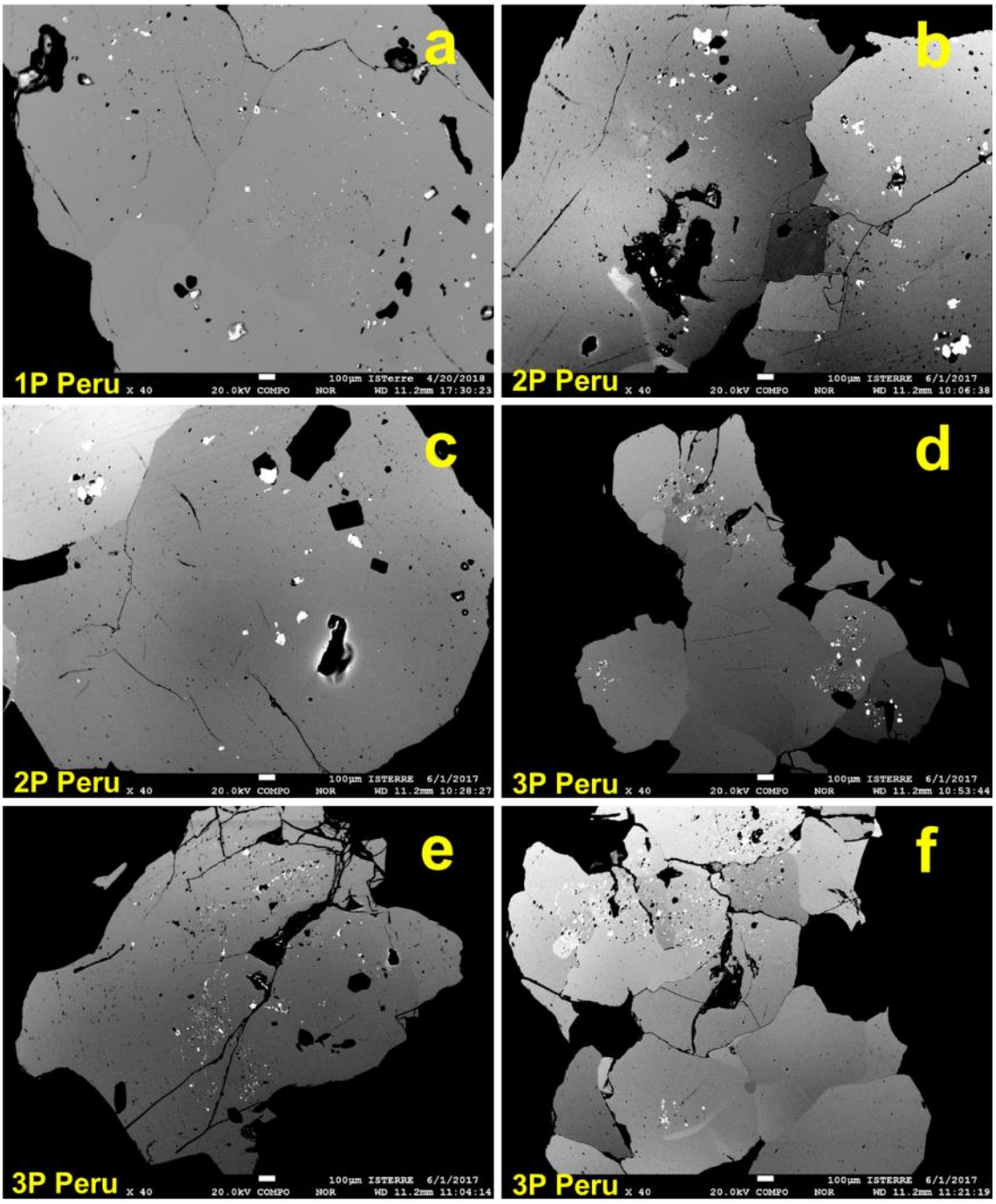


**Figure S3**. BSE images of pyrite with As-rich Cu-sulfide inclusions. Inclusions in (**a**), (**b**), (**d**) and (**e**) have concentric distribution. Distribution of inclusions in (**c**) and (**f**) is unclear most likely because the crystal cuts are not parallel to the growth direction.

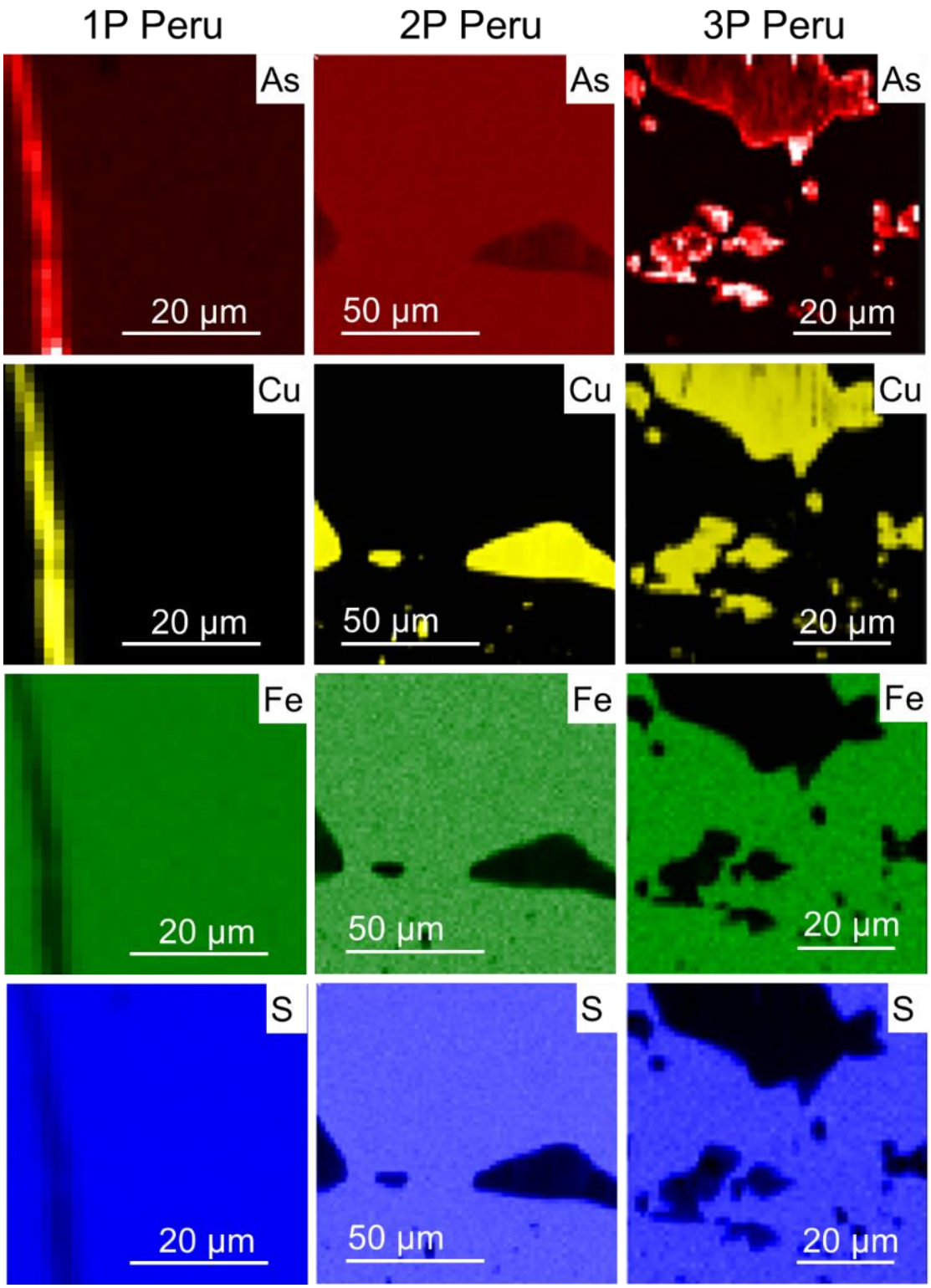


**Figure S4.** EPMA elemental maps. Maps sizes: 1P - 50x50 µm$^2$; 2P - 80x80 µm$^2$; 3P Peru - 60x60 µm$^2$. The pixel size is 1x1 µm$^2$ for 1P and 2x2 µm$^2$ for 2P and 3P. Bright colors correspond to higher element content, darker colors and black correspond to lower element content.

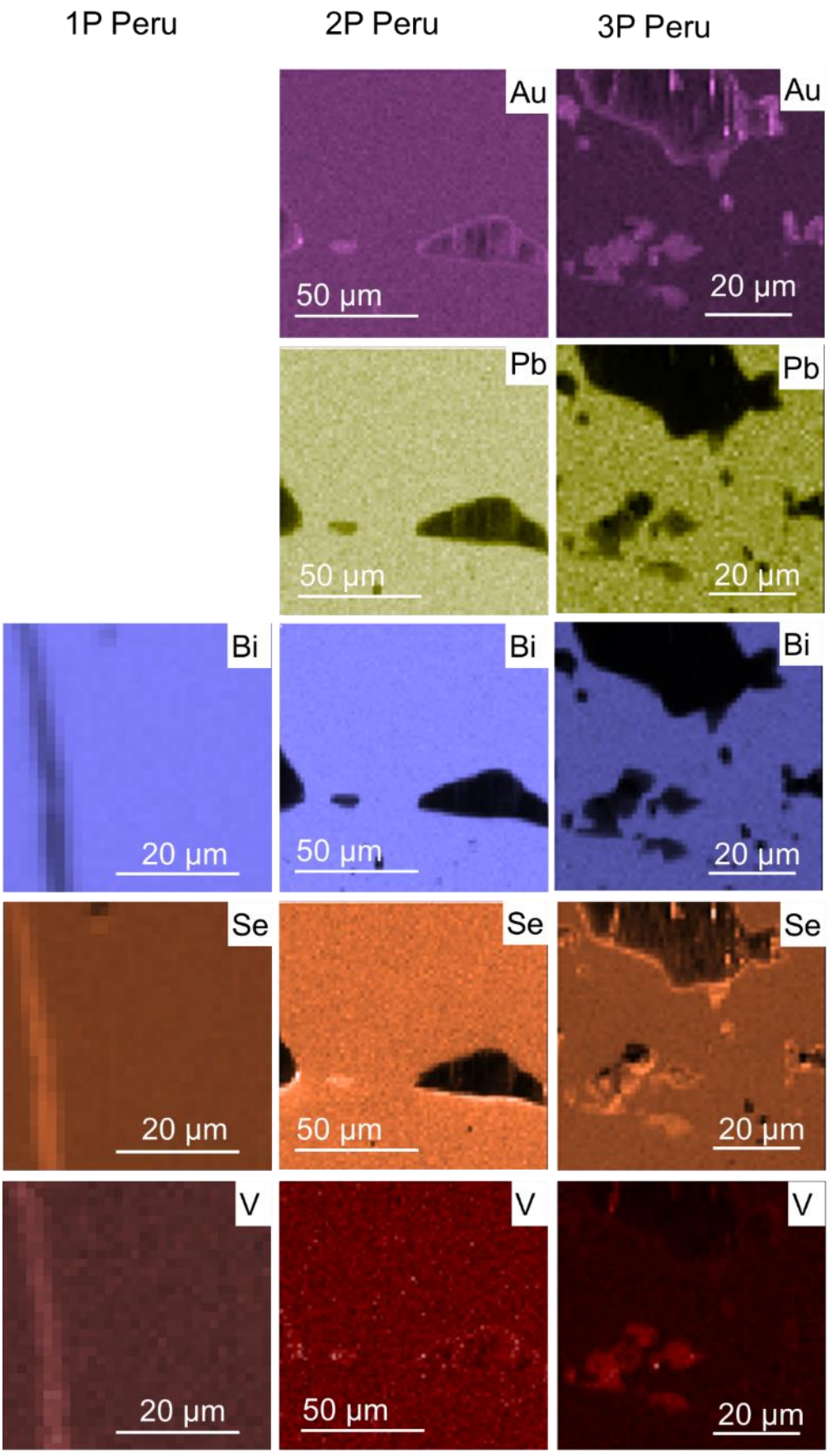


**Figure S5.** EPMA elemental maps of Au, Pb, Bi, Se and V for the three pyrite.

**Scanning electron microscopy (SEM)**

Backscattered electron images and qualitative EDX spectra of inclusions were collected at the ESRF using a field emission scanning electron microscope (SEM) LEO Gemini 1530 (Carl Zeiss, Oberkochen, Germany). Images were acquired with a backscattered electron detector at 10 mm working distance, 30 μm aperture and 20 keV accelerating voltage. EDX spectra of inclusions in pyrite were obtained using X-MAX$^N$ silicon drift detector from Oxford Instruments. The diameter of the electron beam varied from 1 to 100 microns, depending on the inclusions analyzed. Pyrite grains were embedded in epoxy, cross-sectioned, polished, and coated with 10 nm Au. BSE images are shown in Figure S6 and EDX spectra in Figure S7.

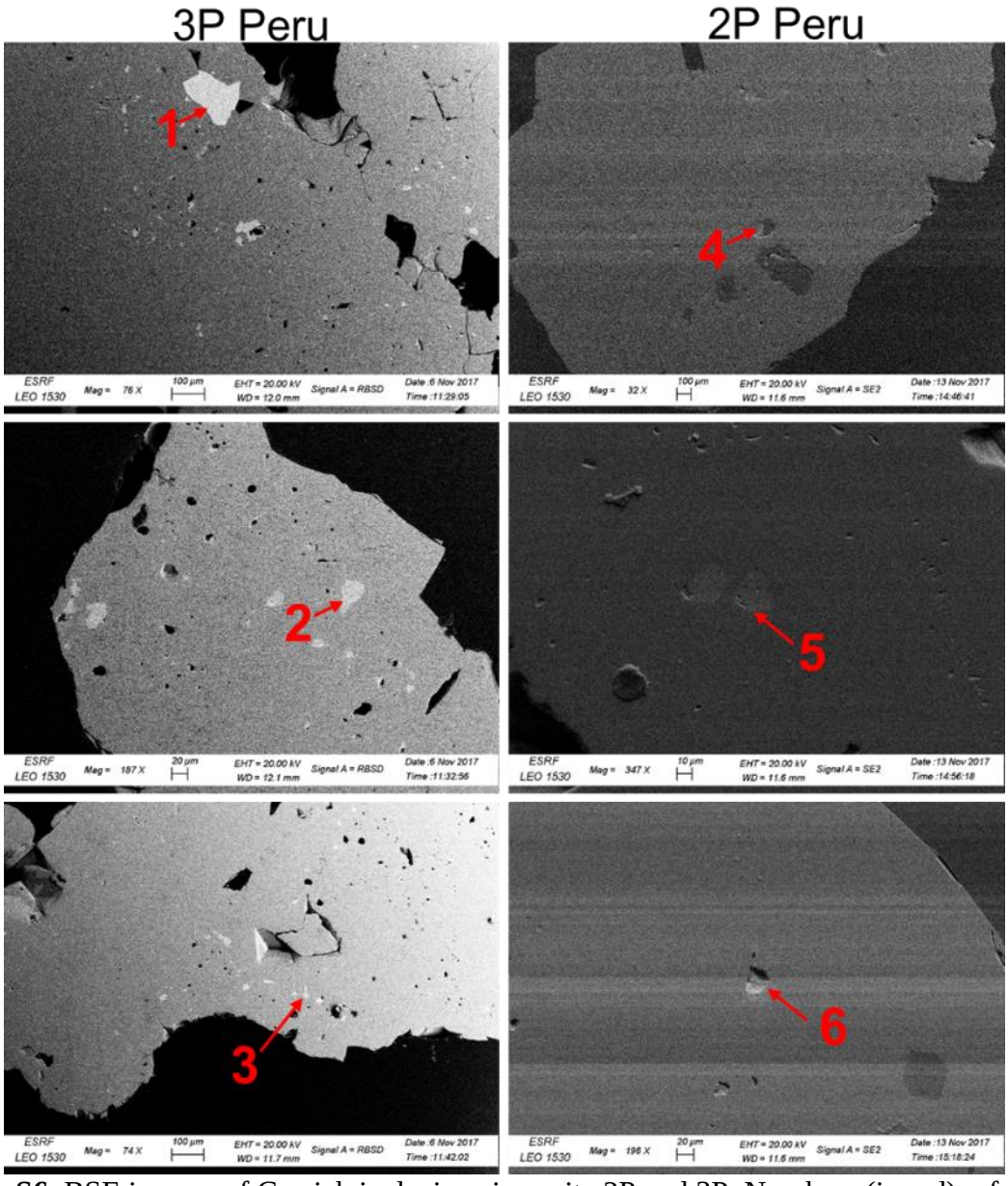


**Figure S6.** BSE images of Cu-rich inclusions in pyrite 2P and 3P. Numbers (in red) refer to the EDS spectra in Figure S7.

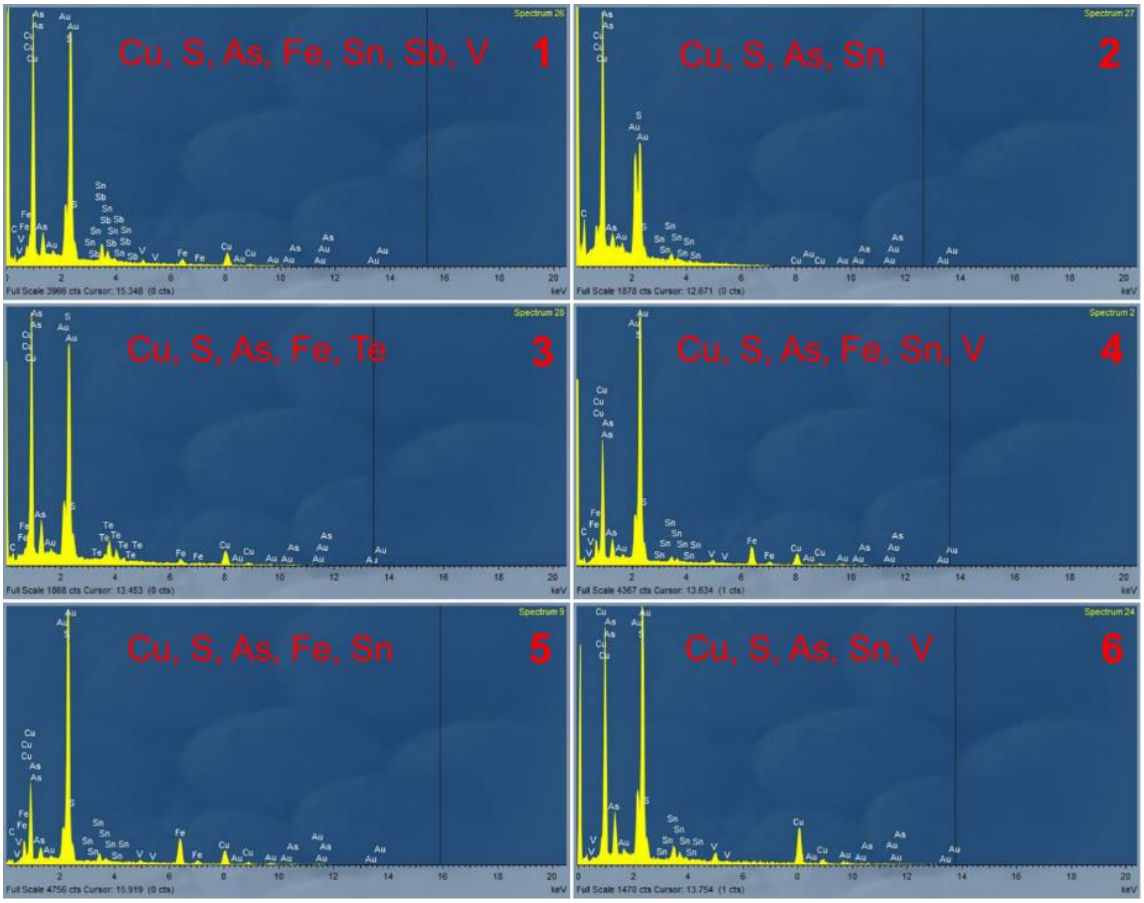


**Figure S7.** EDX spectra of the Cu-rich inclusions shown in Figure S6. The Au peaks are artifact coming from the surface coating. Elements detected by EDX in each analysis are written in red.

**HR-XANES**

The As K-edge HR-XANES spectra were collected on beamline ID26 at the ESRF. A front end Pd-coated mirror with an angle of 2.5 mrad was used to reject higher harmonics. The incoming beam was monochromated with a pair of Si(111) crystals , then focused horizontally by a second Pd-coated mirror and vertically by a third Pd-coated mirror both at 2.5 mrad relative to the incoming beam. The incident monochromatic X-ray beam had a flux of $10^{13}$ photons/sec with a beam size on the sample of 0.2 (V) x 0.7 (H) $mm^2$. The HR-XANES spectra were measured in fluorescence-detection mode with analyzer crystals. The As Kα1 fluorescence line was selected using the 555 reflection of five spherically bent (0.5 m radius; Rovezzi et al. 2017) Si(111) crystals (100 mm diameter) aligned at a Bragg angle of 69.85° in a vertical Rowland geometry. The diffracted intensity was measured with an avalanche photodiode (APD). The combined energy resolution was 2.3 eV. The HR-XANES spectra were measured from 11849 to 11949 eV in continuous scan mode with 0.05 eV step size. The samples were kept at a temperature of 10-15 K using a helium flow cryostat. 50 HR-XANES scans of 20 s were acquired for the As references and 80 scans of 30 s for pyrite. The samples were moved horizontally and vertically after every scan to access unexposed material. No changes in spectral features were noted during the course of data collection that would indicate oxidation of pyrite or other radiation damage. Spectra were averaged with the PyMCA software (Solé et al. 2007) and normalized to a unit step in the absorption coefficient to well above the edge. The absolute energy of the spectra is referenced to the white line energy of $As_2O_3$ taken to 11870.0 eV. The precision of the energy is about ± 0.1 eV. The relative energies between spectra was established by careful comparison of the first derivatives.

**SXRF**

Bulk SXRF measurements of three pyrite (Fig. S8) and micro-SXRF from pyrite 3P (Figs. 3a and S9) were performed on beamline BM23 at the ESRF. The incident beam was monochromated with a pair of Si(111) crystals and focused to 5x5 μm$^2$ with a set of Pt-coated Kirkpatrick-Baez (K-B) mirrors (Mathon et al. 2015) for micro-SXRF. Elemental micro-SXRF maps were obtained by rastering for 2s per point a 12.2 keV incident beam over the sample and measuring the fluorescence signal with a Ketek silicon drift detector (SDD) positioned at 45˚ from the sample. SXRF maps were analyzed with the PyMCA software (Solé et al. 2007).

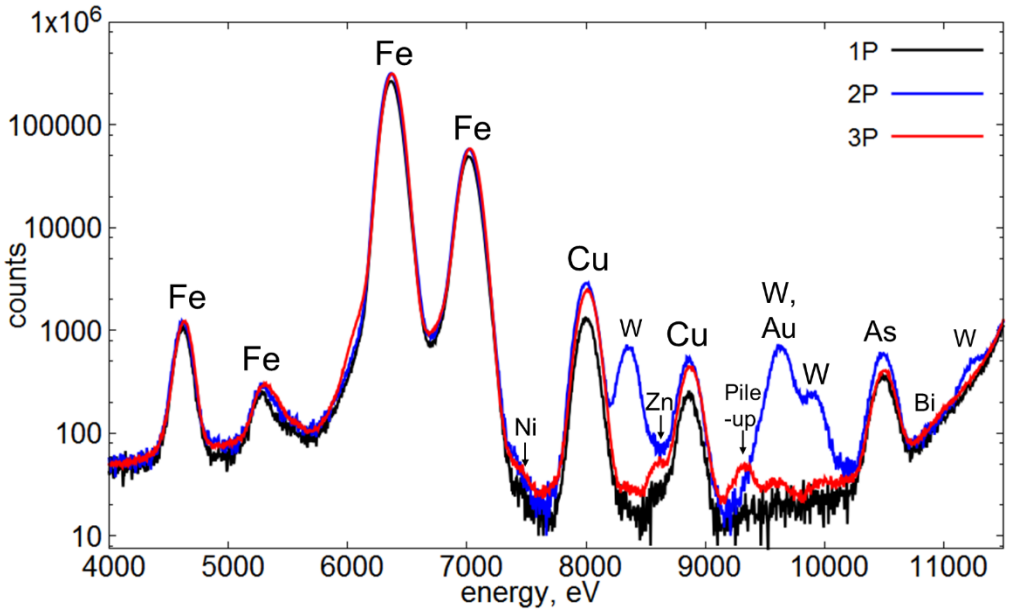


**Figure S8**. Bulk SXRF spectra of 1P, 2P and 3P pyrite. Incident energy, 12.2 keV; collection time, 300 s.

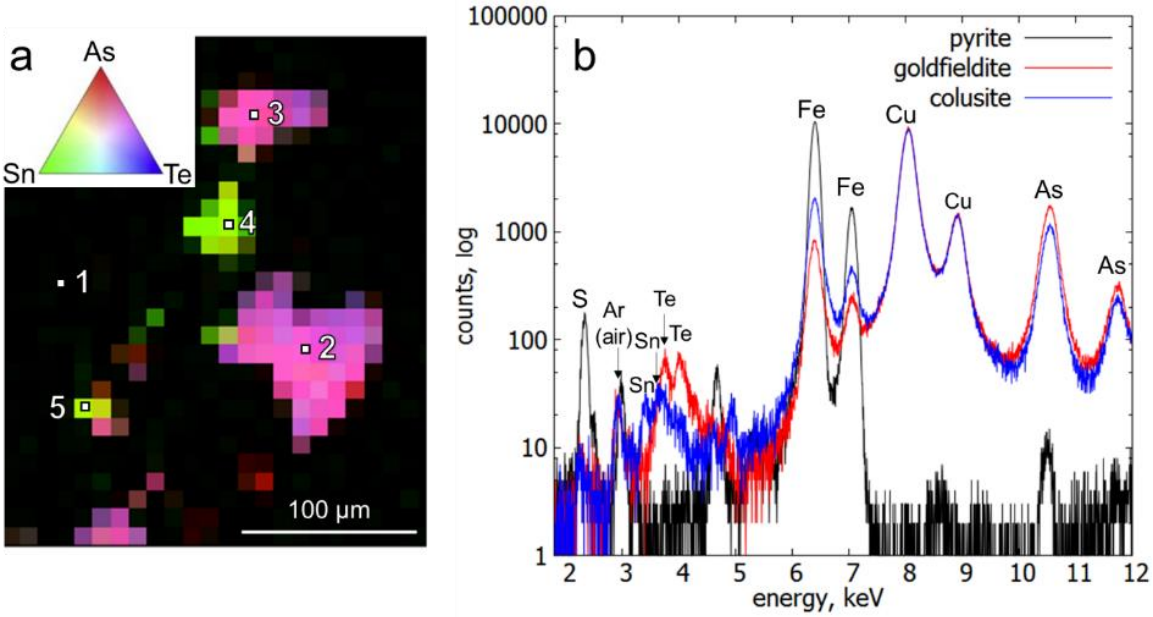


**Figure S9.** (**a**) SXRF map of 3P pyrite. Map size: 240x280 μm$^2$, pixel size: 10x10 μm$^2$; (**b**) Point micro-SXRF spectra measured on the three spots from the SXRF map. Spot1: pyrite; spots 2 and 3: As-goldfieldite; spots 4 and 5: colusite.

**Micro-XANES and micro-EXAFS**

The As K-edge micro-XANES spectra were measured at room temperature with the micro-focus setup of the beamline BM23, a 5x5 $\mu m^2$ beam size, and a Ketek SDD. Points of interest were selected on the SXRF map of pyrite 3P. The incident energy was scanned from 11.75 to 12.15 keV for micro-XANES and to 12.84 keV (16 $Å^{-1}$) for micro-EXAFS measurement. No beam damage was observed. All data were reduced with the Athena software (Ravel and Newville, 2005), and the BM23 and ID26 spectra were intercalibrated on the same energy scale, i.e., 11870.0 eV for the $As_2O_3$ white line. The micro-EXAFS spectra were fit with WinXAS (Ressler 1998) using theoretical amplitude and phase shift functions generated with FEFF7 (Ankudinov and Rehr 1997) using colusite and goldfieldite as structural models. The amplitude reduction factor ($S_o^2$) was kept constant at 0.9, the coordination numbers (CNs) were fixed to their crystallographic values, and the Debye-Waller factor of the S shell optimized and those of the two Cu sub-shells covaried. EXAFS parameters obtained from the fit are detailed in Table S3.

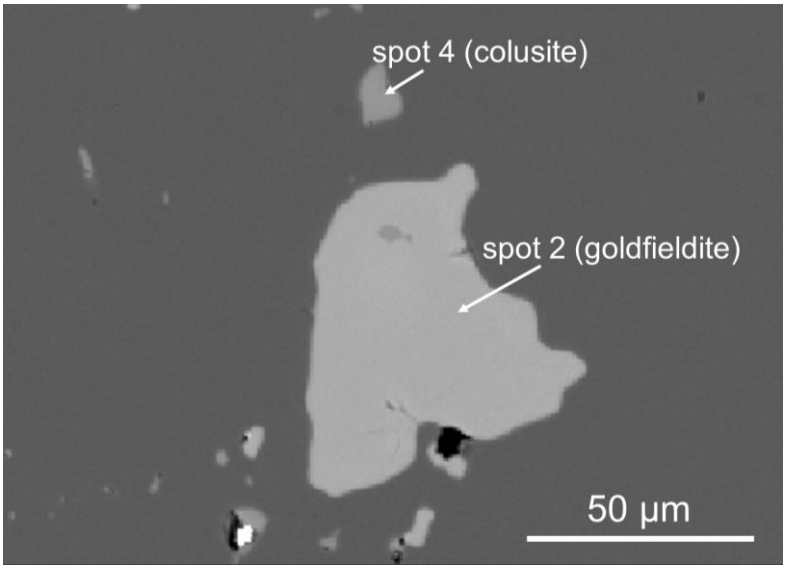


**Figure S10**. BSE image of colusite and goldfieldite inclusions in pyrite 3P. Micro TFY-EXAFS spectra were measured on spots 4 and 2.

**Table S3.** EXAFS parameters from the multi-shell fits of colusite and goldfieldite

| | As-S | | | As-Cu1 | | | As-Cu2 | | | | | |
|---|---|---|---|---|---|---|---|---|---|---|---|---|
| | *CN* | *R* (Å) | σ (Å) | *CN* | *R* (Å) | σ (Å) | *CN* | *R* (Å) | σ (Å) | Δ*E*(eV) | Chi2 | Res |
| Colusite | 4.0[a] | 2.21±0.01 | 0.043±0.024 | 2.7±3.0 | 3.60±0.02 | 0.022±0.062 | | | | 0.1±12.7 | 20865 | 25.9 |
| Colusite | 4.0[a] | 2.23±0.01 | 0.051±0.022 | 7.0±0.3[c] | 3.64±0.01 | 0.048±0.024[b] | 5.0±0.3[c] | 3.81±0.02 | 0.048±0.024[b] | 4.0±5.4 | 13687 | 18.5 |
| Goldfieldite | 3.0[a] | 2.27±0.02 | 0.067±0.012 | | | | | | | 8.2±0.7 | 18765 | 8.0 |

Notes: *CN* is the effective number of atomic pairs seen by EXAFS, *R* is the interatomic distance, σ is the standard deviation of the distance distribution, Δ*E* is the threshold energy correction in eV, and *Res* is the fit residual defined as $[\sum\{|\chi_{exp}-\chi_{fit}|\}/\sum\{|\chi_{exp}|\}]$x100. The many-body amplitude-reduction factor $S_0^2$ was fixed to 0.9. Fit intervals: colusite = 3.7 Å$^{-1}$ ≤ *k* ≤ 15.1 Å$^{-1}$; goldfieldite = 3.7 Å$^{-1}$ ≤ *k* ≤ 12.8 Å$^{-1}$.

[a] Fixed. [b] Constrained to the same value for the two shells. [c] Sum fixed to the crystallographic value of 12.

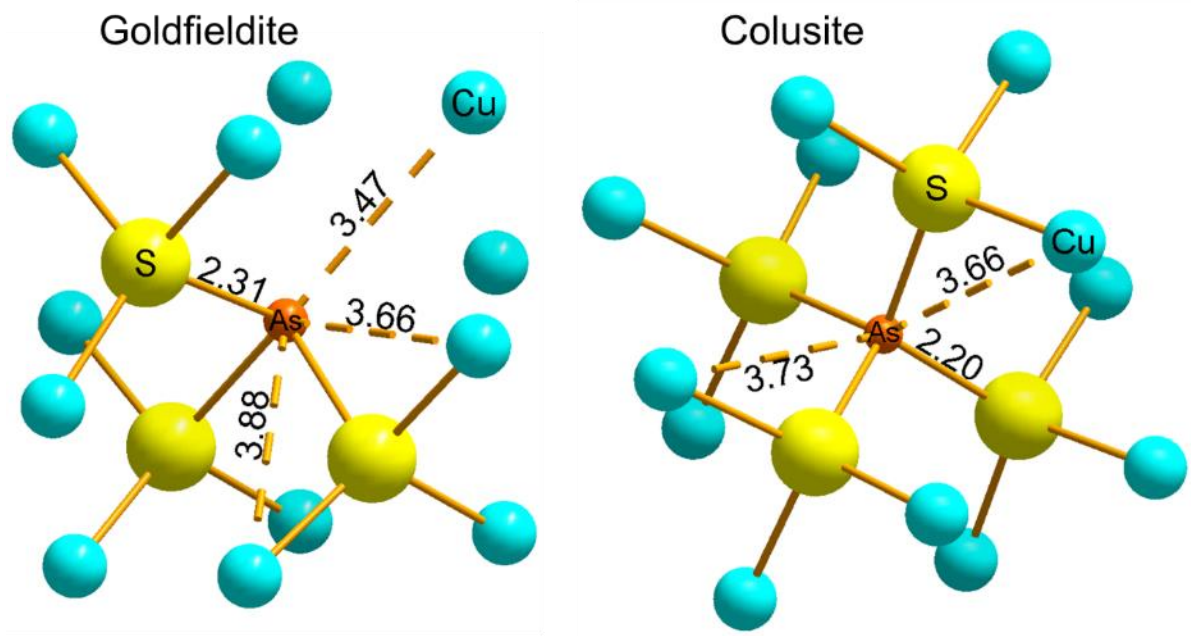


**Figure S11.** Coordination of As in the crystal structures of goldfieldite (Pohl et al. 1996) and colusite (Spry et al. 1994). Numbers are interatomic distances in Å. The As-(S,Cu) distances for goldfieldite are approximative because the site occupancy of As is 0.1 in the refined structure.

**References:**

Ankudinov A. L., and Rehr J. J. (1997) Relativistic calculations of spin-dependent X-ray-absorption spectra. Phys. Rev. B 56, 1712–1716.

Mathon, O., Beteva, A., Borrel, J., Bugnazet, D., Gatla, S., Hino, R., Kantor, I., Mairs, T., Munoz, M., Pasternak, S., Perrin, F., and Pascarelli, S. (2015) The time-resolved and extreme conditions XAS (Texas) facility at the European Synchrotron Radiation Facility: The general-purpose EXAFS bending-magnet beamline BM23. Journal of Synchrotron Radiation. 22, 1548–1554.

Pohl, D., Liessmann, W., and Okrugin, V.M. (1996) Rietveld analysis of selenium-bearing goldfieldites. Neues Jahrbuch für Mineralogie – Monatshefte, 1-8.

Ravel, B., and Newville, M. (2005) ATHENA, ARTEMIS, HEPHAESTUS: data analysis for X-ray absorption spectroscopy using IFEFFIT. Journal of Synchrotron Radiation, 12, 537-541.

Ressler T. (1998) WinXAS: a program for X-ray absorption spectroscopy data analysis under MS-Windows. J. Synchrotron Radiat. 5, 118–122.

Rovezzi, M., Lapras, C., Manceau, A., Glatzel, P., and Verbeni, R. (2017) High energy-resolution x-ray spectroscopy at ultra-high dilution with spherically bent crystal analyzers of 0.5 m radius. Review of Scientific Instruments, 88, 1, 013108.

Solé, V., Papillon, E., Cotte, M., Walter, P., and Susini, J. (2007) PyMCA: a multiplatform code for the analysis of energy-dispersive X-ray fluorescence spectra. Spectrochimica Acta Part B, 62, 63–68.

Spry, P.G., Merlino, S., Wang, S., Zhang, X.M., and Buseck, P.R. (1994) New occurrences and refined crystal chemistry of colusite, with comparisons to arsenosulvanite. American Mineralogist, 79, 750-762.